

ActivationNet: Representation learning to predict contact quality of interacting 3-D surfaces in engineering designs

Rishikesh Ranade^{a,*}, Jay Pathak^a

^a*Ansys Inc., Canonsburg, Pennsylvania, USA*

Abstract

Engineering simulations for analysis of structural and fluid systems require information of contacts between various 3-D surfaces of the geometry to accurately model the physics between them. In machine learning applications, 3-D surfaces are most suitably represented with point clouds or meshes and learning representations of interacting geometries from point-based representations is challenging. The objective of this work is to introduce a machine learning algorithm, *ActivationNet*, that can learn from point clouds or meshes of interacting 3-D surfaces and predict the quality of contact between these surfaces. The *ActivationNet* generates activation states from point-based representation of surfaces using a multi-dimensional binning approach. The activation states are further used to contact quality between surfaces using deep neural networks. The performance of our model is demonstrated using several experiments, including tests on interacting surfaces extracted from engineering geometries. In all the experiments presented in this paper, the contact quality predictions of *ActivationNet* agree well with the expectations.

1. Introduction

Many applications in engineering simulation & robotics involve geometries with a large number of 3-D surfaces and a non-trivial interaction between them. The goal of engineering simulation is to predict the underlying physics present in a physical system or process. In many cases, the accuracy of these predictions is predicated on the contact between the various 3-D surfaces in the geometry. As a result, it is important to identify the contact quality of all the interacting 3-D surfaces in a geometry so as to effectively model the physical phenomenon resulting from their interactions.

Engineering simulation software, such as Ansys, use contact detection algorithms [1, 2, 3, 4, 5, 6] to identify all possible contacting surfaces in a given 3-D geometry. Due to algorithmic limitations, most of these methods only identify

*Corresponding Author.: Email Address: rishikesh.ranade@ansys.com (R.Ranade)

the interacting surfaces in the geometry but cannot separate surfaces with good contacts from bad. Surfaces with bad contact are undesirable and generally hamper the accuracy and convergence of physics-based solvers. Hence, it is necessary to prune these contacts before running the simulations.

In engineering applications, the contact between 3-D surfaces is generally characterized by handcrafted features such as, proximity, solid angle and overlap. Proximity refers to the distance between the interacting surfaces, solid angle is the angle between them and overlap denotes the intersection between these surfaces. In general, 3-D surfaces with good contact should have a smaller proximity and angle but a larger overlap. Although, the computation of these features is extremely expensive and in some cases not possible at all, especially for arbitrarily shaped 3-D surfaces with curvy and intricate geometries. Additionally, each side of the contacting surfaces may be a collection of many surfaces which further adds to complexity of defining a good contact. Moreover, even if these features could be evaluated, it is very difficult to devise a metric for a contact quality score that includes a combination of these features, since the correlation between them may be non-linear depending on the size and shape of the 3-D surfaces. As a result, expert design modelers need to intervene and manually separate surfaces with good contacts from bad, solely based on experience and prior knowledge. In this context, machine learning strategies can be very useful in informing the design modelers on the nature and quality of the various contacting surfaces present in 3-D geometries, and save computational time and resources.

In recent times, Machine Learning (ML) algorithms have made significant progress in learning and representing complicated 3-D surfaces. The initial efforts in learning from 3-D geometries were made by developing and employing 3-D Convolutional Neural Networks (CNNs) [7, 8, 9]. These approaches worked with voxelized representations of geometries. As a result, they were prone to data sparsity and memory constraints. Research works following this tackled these challenges by representing 3-D surfaces and parts with point clouds and meshes. In the context of engineering computer aided design (CAD), 3-D geometries are generally represented using standard triangle language (STL). Point clouds represent the x, y, z coordinates of nodes of the triangles representing the surfaces. On the other hand, meshes are represented by coordinates of mesh nodes as well as the adjacency relationship between them. The main advantage of point clouds and meshes is in their unstructured data structure, which can effectively represent the most intricate features of the 3-D geometry. However, feature extraction from these unstructured representations has proven to be challenging for deep learning algorithms. As a result, traditional approaches to feature extraction from point clouds relied on hand-crafting these features [10, 11, 12, 13, 14, 15, 16, 17, 18, 19]. The extracted features encode statistical information and are designed to be invariant to certain transformations. In recent years, other approaches of converting point clouds and meshes to voxel-based structured representations have been explored [20, 21, 22, 23, 24]. The voxel-based representations allow feature extraction using the already matured CNN-based network architectures, but these approaches are memory intensive,

especially for 3-D data sets. Other alternative approaches include using multi-view image representations of point cloud [25, 26, 27, 28, 29, 30]. Multi-view CNNs provide a better performance than voxel-based approaches but lose accuracy in the stitching process. More recently, CNNs have also been extended with multi-resolution voxel representation to efficiently handle memory requirements in encoding and decoding 3-D geometries [31, 32]. The advent of new modeling approaches such as PointNet [33], PointNet++ [34] and graph CNNs [35, 36, 37, 38, 39] provide an opportunity to learn features directly from point cloud and mesh representations and have applications in tasks involving classification, segmentation and detection. However, to the knowledge of the authors, the research work using these methods has focused on extracting features from geometries of single 3-D parts, and has never been applied to evaluate the interactions between multiple contacting 3-D surfaces.

In this work, we introduce the *ActivationNet*, which is a machine learning algorithm that uses coarse point cloud or mesh representations of interacting 3-D surfaces and predicts a contact quality score associated to the surface pair. The *ActivationNet* uses voxel-based methodologies to pre-process the interacting 3-D surface points and compute activation states using a multi-dimensional binning strategy [40]. The activation states are based on the spatial location and density of points, represented either by point clouds or mesh nodes, in a normalized 3-D space. The activation states provides neural networks the opportunity to extract features which are equivalent to the hand-crafted features such as proximity, angle and overlap. It also takes into account the important and intricate characteristics of 3-D surfaces, that are useful for learning surface interactions. A detailed explanation of the meaning and construction of activation states as well as a description of the network architecture of *ActivationNet* has been provided in Section 2 of this paper.

The rest of the paper is organized as follows. In section 2, we describe the *ActivationNet* in great detail and describe the generation of activation states. This is followed by a description of the data generation process and the training mechanics. The *ActivationNet* is validated on several interacting 3-D surfaces extracted from unseen 3-D geometry models of engineering objects. The results from the *ActivationNet* are compared with those from PointNet to showcase the ability of the *ActivationNet* to learn representations and extract features from point clouds of 3-D surfaces, to predict contact quality with a very high accuracy.

The key contributions of our work are as follows:

- We propose a machine learning methodology, *ActivationNet* to extract features from interacting point clouds to predict a contact quality score.
- We demonstrate that *ActivationNet* learns true representations which are useful in making intuitive predictions and it is not just overfitting data.
- Furthermore, our approach is demonstrated for predicting contact quality on actual engineering geometries used in engineering simulations pertaining to structural analysis.

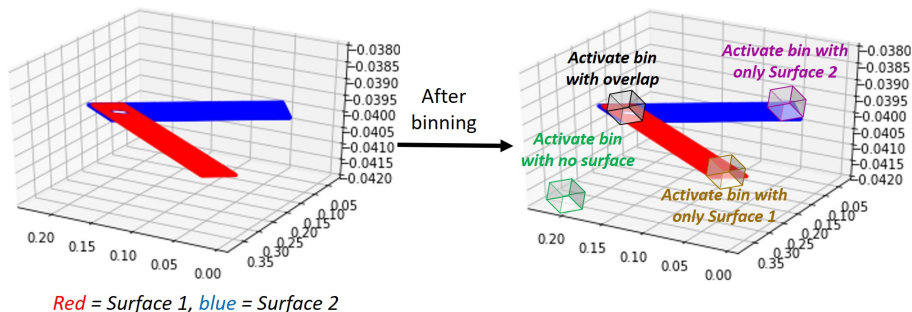


Figure 1: Activation state using multi-dimensional binning

2. *ActivationNet*: Model formulation

ActivationNet is a machine learning algorithm that predicts contact quality from point-based representations of interacting 3-D surfaces. The point-based representation is an unavoidable starting point for our algorithm because all engineering simulations use either point clouds or meshes to represent 3-D geometries. As stated previously, representation learning from discrete points is challenging, and hence we extract features not directly from these points but from the activation states, which are derived from them.

Activation states are constructed using the multi-dimensional binning approach. Starting from discrete points representing interacting surfaces, the binning approach divides the 3-dimensional space occupied by these points into smaller bins of uniform size and shapes. This process is similar to voxelization except that, each bin is characterized by the number of points it contains and information regarding the interacting surface they belong to. These bin characteristics are used to determine an activation state for each bin. Figure 1 describes the construction of activation states in more detail. In Figure 1, the surface 1 is represented by a dense cloud of points marked red, while the surface 2 is represented by points marked blue. The multi-dimensional binning approach divides the space surrounding the point clouds into smaller cube boxes. The bounds of the surrounding 3-D space are determined based on the span of the coordinates of the points. As mentioned earlier, each bin is associated an activation state based on the characteristics of the bin. For example, a bin containing points from only surface 1 is given an activation state, say 1, while a bin with points from only surface 2 is given an activation state, say 2. On the other hand, bins with points from both surfaces are considered to be bins representing overlapping regions of the interacting surfaces, and are given a different activation state, say 3. Finally, bins with points from neither surfaces are simply activated with 0. Moreover, this can be easily extended to scenarios with more than 2 interacting surfaces. In such cases, the binning procedure would remain the same, but the activation states would also take into account the interaction between all the pairs of different surfaces. To that end, the activation states

on each bin implicitly represent the extent of overlapping regions, based on the number of overlapping bins for a given sample, proximity and angle between the surfaces, based on the proximity and orientation of a given bin with respect to other bins. Thus, activation states provide neural networks the opportunity to directly extract these features and estimate contact quality.

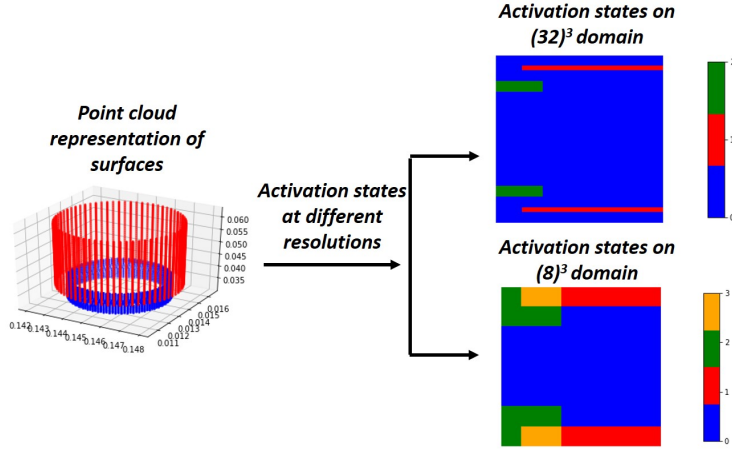


Figure 2: Multi-resolution activation states

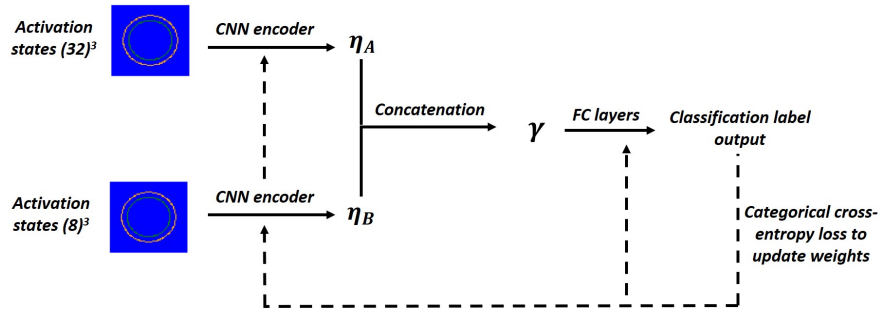


Figure 3: Neural network architecture

It may be important to note that the features represented by activation states depends on the choice of bin size in the multi-dimensional binning approach. Larger bin sizes will extract coarser features of surface interaction as opposed to smaller bins, which will focus more on the finer and intricate features. Features from both representations may be necessary to accurately predict the quality of surface interactions. Figure 2 shows a 2-D cut plane drawn at an intercept of 0.04 in the vertical direction. It may be observed that the lower resolution bins have a coarser representation, while the finer resolution bins have a much

crisper representation. Both coarser and finer representations are important to understand the relative position of the interacting surfaces with each other. For example, in Figure 2, the partial overlap in the coarser resolution indicates that the interacting surfaces may have a projected overlap but the finer resolution does not capture this feature but focuses more on the distance between the two surfaces. In many cases, the interplay between the projected overlap and proximity can influence the overall quality of the contacting surfaces.

Thus, the activation states at multiple resolutions are used as inputs in the neural network. Figure 3 shows a schematic diagram of the neural network architecture used in this work. First, the multi-resolution activation states are encoded using convolutional layers. The network uses a combination of convolutional layers followed by pooling layers to extract features at different spatial resolutions. The final convolutional layer at the smallest spatial resolution is flattened to determine an encoding for each activation states. The encoding of the higher resolution activation state is represented by η_a , while the lower resolution activation state is represented by η_b . The size of the encoding vectors may be different for different resolutions. The encoding of activation states may capture a combination of features such as proximity, angle and overlap but are not limited to that. The activation states’ encodings are concatenated and passed through fully connected deep layers. Both convolutional and fully connected layers use a ReLU activation function. Moreover, all the convolutional layers are followed by batch normalization layers [41] and the fully connected layers by dropout layers [42]. The output layer of the network predicts the class probability and hence has a sigmoid activation. This problem is setup as a three class problem, where the class label 1 refers to good contacts (with a quality score of 100), class label 2 refers to bad contacts (with a quality score of 0) and class label 3 refers to neutral contacts (with a quality score of 50), which are neither good nor bad and have a quality of somewhere in between. Finally, a heuristic computation of contact quality score is designed based on the class probabilities predicted by the neural network. The contact quality score for a given pair of interacting surfaces is shown below in equation 1.

$$C = P(1) * 100.0 + P(2) * 0.0 + P(3) * 50.0 \quad (1)$$

where, C is the contact quality score and P is the class probability.

A three class problem was found to be very suitable for this application because the contact quality calculation is based on the class probabilities of network output. A two-class problem might bias the contact quality prediction in one direction or the other. The third class puts the quality score on a spectrum and accommodates for interacting 3-D surfaces whose contact quality is neither good or bad and depends largely on the application.

Since this problem is set up as a three-class classification problem, we use a categorical cross-entropy loss to update the network weights. The training is carried out using TensorFlow using a mini-batch Adams optimizer. The training is started with a learning rate of $1e^{-3}$ and a learning rate scheduler is used to modulate the learning rate depending on the validation losses. In Section, 3, we discuss the data generation and annotation in more detail.

3. Data generation and annotation

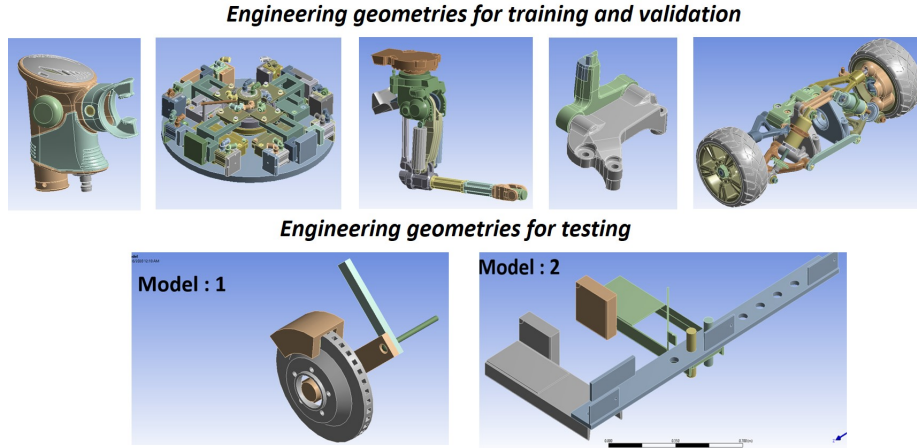


Figure 4: Engineering geometries used for creating training, validation and testing datasets

The training and validation data for our network consists of 3-D interacting surfaces extracted from 5 CAD models of engineering geometries, while the testing data consists of surfaces extracted from 2 different CAD models. We use the Ansys software suite to model the engineering geometries. Figure 4 shows the engineering geometries used for generating the data. On each engineering geometry, we use a contact detection algorithm to identify all possible contacting 3-D surfaces. The algorithm uses a proximity-based single gap tolerance to identify surfaces that will be considered to be in contact. The gap tolerance itself is heuristically determined using a fraction of largest diagonal of all bodies in the CAD model. Since the contact detectors are not good at identifying contacts with good quality, ML algorithms such as the one proposed in this work, *ActivationNet*, are extremely useful in accurately predicting contact quality, such that contacts with bad quality can be easily eliminated.

Since, there is no explicit calculation for determining the contact quality score for arbitrary 3-D interacting surfaces, the training, validation and testing data is annotated by assigning a score range (between 0 and 100) based on visual inspection with guidance from experts in engineering simulation. The range of quality score assigned by expert modelers varies within 10 points. In this work, the score ranges for each pair of 3-D surfaces are averaged over evaluations from 10 expert design modelers. The averaged score range is used to assign a class label for all 3-D interaction surfaces. We assign samples to,

- class 1, if score ≥ 80
- class 2, if score ≤ 20
- class 3, if score ≥ 20 and ≤ 80

The 3-D interacting surfaces are represented by discrete points, which are generated meshing the surfaces with coarse triangular meshes and extracting the nodal coordinate information. Sampling techniques may be used to generate more points within each triangular element if a higher resolution is required. The nodes of the triangular elements as well as any sampled points are used as point-based representations and are provided as inputs to the *ActivationNet* algorithm described in Section 2. The point representations of 3-D surfaces extracted from 5 engineering geometries and their associated class labels are split into training and validation datasets, such that 75% is reserved for training and the rest for validation. There are only 300 contacting surfaces extracted from the 5 engineering geometries. Data augmentation techniques to rotate point clouds along planes in x, y, z directions are used to increase the training data. On the other hand, as mentioned previously, 3-D surfaces extracted from completely new engineering geometries, which our model has never seen before, are used for testing purposes.

4. Results & discussions

In this section, we demonstrate the trained *ActivationNet* for several cases and scenarios. In the first set of experiments, the goal is analyze whether the *ActivationNet* is truly learning surface interactions and not just overfitting the training data set. The training data set consists of only 300 arbitrarily shaped contacting surfaces from 5 engineering geometries and hence, this experiment is crucial to prove the representational learning capability of our method. To that end, in this experiment we conduct demonstrations on simpler, interacting 3-D surfaces. These surfaces are translated, rotated and scaled relative to one another and the predictions obtained from the *ActivationNet* are evaluated to prove that our approach is learning valid representations. In the next set of experiments, we demonstrate the *ActivationNet* on 3-D surfaces extracted from the 2 engineering geometries, that are reserved for testing. In this experiment, we also compare our results with the PointNet [33] algorithm for computation using point clouds.

4.1. Translation of point clouds of 3-D surfaces

In this study, we evaluate the predictions of *ActivationNet* for translation of 3-D surfaces with each other. Intuitively, as 3-D surfaces move away from each other, the contact between them reduces. The goal of this study is to analyze the consistency of the *ActivationNet* with respect to this observation. In Figure 5, we show two surfaces which are initially in contact with each other and subsequently are pulled apart. The corresponding contact quality score predicted by our model is also shown in Figure 5. It may be observed that initially when the surfaces are in contact with each other, the predicted quality score is 17.22. The predicted contact score is relatively low, because, even though the surfaces are close to each other, the overlapping regions are small. Nonetheless, as the surfaces move further away from each other, the contact

score predictions significantly drop and almost reach close to 0 in the most extreme case.

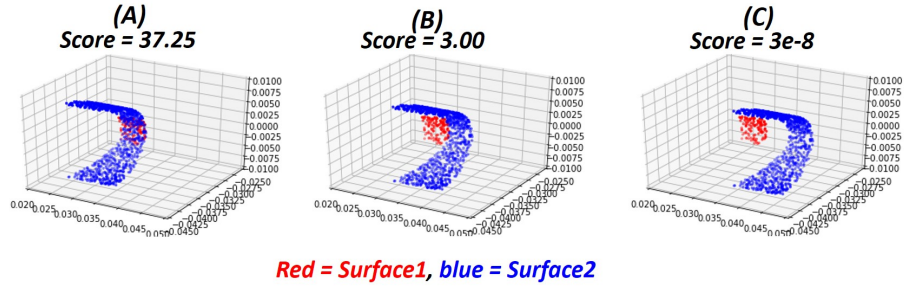


Figure 5: *ActivationNet* predictions for translation of 3-D surfaces

4.2. Rotation of point clouds of 3-D surfaces

In the next experiment, we rotate the point clouds of 3-D surfaces with respect to one another and validate the performance of our model. It may be observed from Figure 6, that the surfaces, initially, have the same size and are exactly on top of each other. The prediction of *ActivationNet* is a contact score of 100 because the angle between the surfaces is 0° and there is 100% overlap between the surfaces. As the angle between the surfaces is increased, the overlapping regions between the surfaces changes from a surface contact to a line contact, and contact quality score prediction drops. The predicted score is the smallest when the surfaces are perpendicular to one another.

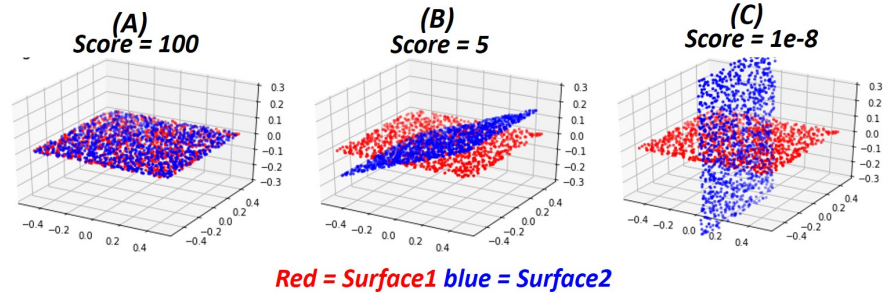


Figure 6: *ActivationNet* predictions for rotation of 3-D surfaces

4.3. Scaling of point clouds of 3-D surfaces

In this experiment, we scale the point clouds of 3-D surfaces with respect to one another and validate the performance of our model. It may be observed

from Figure 7, that the surfaces initially have the same size and there is 100% overlap between them. Subsequently, the size of surface 1 is kept the same but the size of surface 2 is reduced by a factor of 2. When the surfaces have the same size, the contact quality score is 100 due to the strong overlap. Moreover, the contact quality score reduces by the same factor as the size of the second surface. As the size of surface 2 is made smaller, the overlapping region between the surfaces reduces and the contact quality score prediction drops by the same factor. The predictions from *ActivationNet* agree well with the expectation.

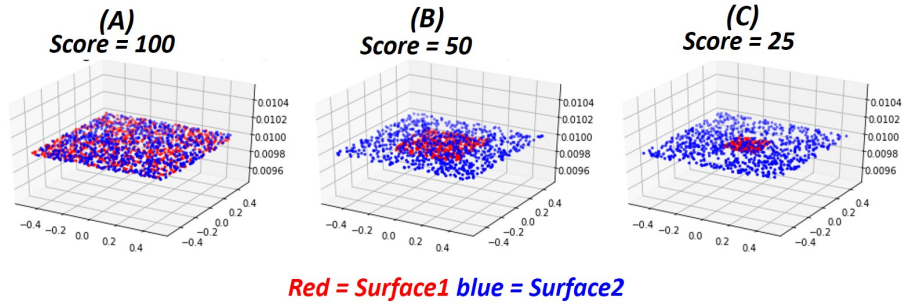


Figure 7: *ActivationNet* predictions for scaling of 3-D surfaces

4.4. Testing on unseen engineering geometries

It is evident from the previous experiments that the *ActivationNet* is learning the true representation of interactions between arbitrary 3-D surfaces. Next, we test the model on interacting surfaces generated from 2 engineering geometries. The engineering geometries used for testing are shown in Figure 4 and the surfaces on these geometries are not seen by our model during training. The 3-D interacting surfaces are generated using a contact detection algorithm and a coarse triangular mesh is generated on all the surfaces. A sampling technique is implemented to sample 10 points on each triangular element of the coarse mesh. 14 interacting surfaces are extracted from testing geometry 1, while, 10 interacting surfaces are extracted from testing geometry 2. The contact quality predictions for these surfaces are carried out using *ActivationNet* and PointNet [33]. The samples used for testing are annotated by engineering simulation experts, such that the contact quality score falls in a specified range. The goal for both the methods is to predict contact quality scores, which fall within the expected range.

Figure 8 shows selected results obtained on the interacting surfaces obtained from testing geometry 1. It may be observed that for all cases, the contact quality score prediction of our model fall within the expected range of the score assigned by expert design modelers. For test samples *A*, *E* and *F*, the expected score ranges between 90 and 100, because the interacting surfaces have the same size and are positioned with a 100% overlapping between them. Our

model is able to extract features to understand this and provide a suitable score. On the other hand, test samples C and D have concentric surfaces with no contact between them. Our model predicts a very low score of $1e^{-8}$ and $1e^{-6}$, respectively, which is also expected for these samples. For test samples, B , the surfaces are at a 45° angle with respect to one another and there is some overlap near the top of the surface. As a result, our model predicts a score of 48.5 for this sample. All in all, the predictions obtained from the *ActivationNet* are reasonable and reliable for testing geometry 1 and agree well with the expected range specified by the experts modelers.

Next, we observe some of the results obtained on the interacting surfaces obtained from testing geometry 2. The results may be observed in Figure 9. It may be observed that for all cases, the contact quality score prediction of our model falls within the expected range provided by the experts. For test samples A and D , the expected score ranges between 0 and 10, because the contact between the surfaces is a line contact. The features extracted by our model is able to understand this and provide a suitable score. On the other hand, test samples F has a relatively bigger overlapping region and hence our model predicts a score of about 50, which was also expected for this sample. For test samples, B and C , the surfaces are very close to one another and there is a good amount of overlap. There is 100% overlap from the perspective of the surface represented by red but lesser from the perspective of the blue surface. Our model is able to capture these representations and predicts a score of 50 for both these test samples. Moreover, sample B is a flipped version of sample C , but the nature of contact between them is very similar. Our model can capture this and is able to make accurate and reasonable predictions. Similarly, in sample E , where the blue concentric surfaces has a 100% overlap with the red surface but the red surface is larger and the percentage of overlap maybe smaller. The proximity between the surfaces is small. Hence, the predicted contact quality score is 47.95. Overall, the predictions obtained from the *ActivationNet* are reasonable and reliable for both testing geometry’s 1 and 2 and agree well with the expected range specified by the experts.

Finally, we compare the results of *ActivationNet* with those obtained from PointNet [33]. The PointNet is set up such that the point clouds from the two interacting surfaces are labeled with surface identifiers, so as to distinguish between the surfaces. In our experience, from the context of learning interactions between surfaces, it is very important to associate identifiers with the surfaces to achieve better performance with PointNet. As mentioned earlier, the network architecture for PointNet is designed to solve a 3-class classification problem. The description of class definitions is provided in section 3. The contact quality score is evaluated using Equation 1 on 24 interacting surfaces obtained from the 2 test geometries using both PointNet and *ActivationNet*. The comparisons are shown in Tables 1 and 2. It may be observed that the *ActivationNet* is effective and accurate at predicting interactions between contacting 3-D surfaces.

Surface Id	<i>ActivationNet</i>	PointNet	Expected
1	49.99	4.79	40-50
2	100	84.69	90-100
3	1e-6	0.11	0-10
4	1e-6	0.18	0-10
5	1e-8	0.02	0-10
6	49.004	6.99	40-50
7	49.004	6.17	40-50
8	100	78.18	90-100
9	100	78.83	90-100
10	48.5	0.48	50-60
11	100	58.46	90-100
12	100	99.34	90-100
13	100	53.91	90-100
14	100	99.71	90-100

Table 1: Comparison of contact quality scores between *ActivationNet* and PointNet on different surfaces of test geometry 1

Surface Id	<i>ActivationNet</i>	PointNet	Expected
1	4.18	49.82	0-10
2	7.93	49.32	0-10
3	0.002	65.96	0-10
4	47.95	49.92	40-50
5	50.0	7.71	40-50
6	47.75	15.4	40-50
7	3.75	39.31	0-10
8	50	49.84	40-50
9	50	49.74	40-50
10	16.74	65.82	0-10

Table 2: Comparison of contact quality scores between *ActivationNet* and PointNet on different surfaces of test geometry 2

5. Conclusion

In this paper, we introduce a machine learning algorithm, *ActivationNet*, to extract features from point-based representations of interacting 3-D surfaces and provides a score for contact quality. Many applications in engineering simulation require information of contact quality to accurately solve physics. The traditional algorithms that can process points have not been designed to capture such interactions. Our model is geared toward such applications and provides an opportunity to effectively predict quality of contacts, thereby eliminating human intervention and saving computational time and resources in engineering simulations.

ActivationNet processes point-based representations of interacting surfaces and generates activation states using a multi-dimensional binning approach. The activation states are generated at multiple resolutions of bins. The multi-resolution activation bins are inputs to our neural network which is a classification based algorithm. The class probabilities are used to predict a contact quality score using a heuristic model.

Finally, the *ActivationNet* has been tested over several test cases. The first set of experiments are designed to prove that the *ActivationNet* is learning true representations of interacting surfaces and not just overfitting the training data. This is followed by demonstrations on interacting surfaces generated from actual engineering geometries, which were not seen during training. The results of this experiment are compared with the well-known PointNet algorithm. The results from our algorithm are shown to agree well with the expected results for various interacting surfaces with arbitrary shapes and size, that were part of the testing geometries.

References

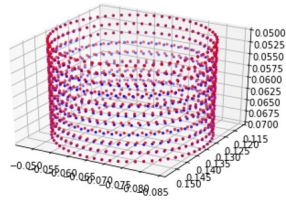
- [1] M. Heinstein, S. Attaway, J. Swegle, F. Mello, A general-purpose contact detection algorithm for nonlinear structural analysis codes, Tech. rep., Sandia National Labs., Albuquerque, NM (United States) (1993).
- [2] A. Munjiza, D. Owen, N. Bicanic, A combined finite-discrete element method in transient dynamics of fracturing solids, *Engineering computations* (1995).
- [3] A. Munjiza, K. Andrews, J. White, Combined single and smeared crack model in combined finite-discrete element analysis, *International journal for numerical methods in engineering* 44 (1) (1999) 41–57.
- [4] E. Rougier, Discrete element method for simulation of gas micro-flows, Ph.D. thesis, Queen Mary, University of London (2009).
- [5] A. A. Munjiza, E. E. Knight, E. Rougier, *Computational mechanics of discontinua*, John Wiley & Sons, 2011.
- [6] G. G. Schiava d’Albano, A. Munjiza, T. Lukas, Novel ms (munjizaschiava) contact detection algorithm on multicore pc, in: *PARTICLES III: proceedings of the III International Conference on Particle-Based Methods: fundamentals and applications*, CIMNE, 2013, pp. 35–45.

- [7] D. Maturana, S. Scherer, Voxnet: A 3d convolutional neural network for real-time object recognition, in: 2015 IEEE/RSJ International Conference on Intelligent Robots and Systems (IROS), IEEE, 2015, pp. 922–928.
- [8] L. Yi, V. G. Kim, D. Ceylan, I.-C. Shen, M. Yan, H. Su, C. Lu, Q. Huang, A. Sheffer, L. Guibas, A scalable active framework for region annotation in 3d shape collections, *ACM Transactions on Graphics (ToG)* 35 (6) (2016) 1–12.
- [9] C. R. Qi, H. Su, M. Nießner, A. Dai, M. Yan, L. J. Guibas, Volumetric and multi-view cnns for object classification on 3d data, in: Proceedings of the IEEE conference on computer vision and pattern recognition, 2016, pp. 5648–5656.
- [10] E. Grilli, F. Menna, F. Remondino, A review of point clouds segmentation and classification algorithms, *The International Archives of Photogrammetry, Remote Sensing and Spatial Information Sciences* 42 (2017) 339.
- [11] A. E. Johnson, M. Hebert, Using spin images for efficient object recognition in cluttered 3d scenes, *IEEE Transactions on pattern analysis and machine intelligence* 21 (5) (1999) 433–449.
- [12] H. Chen, B. Bhanu, 3d free-form object recognition in range images using local surface patches, *Pattern Recognition Letters* 28 (10) (2007) 1252–1262.
- [13] Y. Zhong, A shape descriptor for 3d object recognition, in: Proceedings ICCV 2009 Workshop 3DRR, Vol. 6, 2009.
- [14] R. B. Rusu, N. Blodow, Z. C. Marton, M. Beetz, Aligning point cloud views using persistent feature histograms, in: 2008 IEEE/RSJ international conference on intelligent robots and systems, IEEE, 2008, pp. 3384–3391.
- [15] R. B. Rusu, N. Blodow, M. Beetz, Fast point feature histograms (fpfh) for 3d registration, in: 2009 IEEE international conference on robotics and automation, IEEE, 2009, pp. 3212–3217.
- [16] F. Tombari, S. Salti, L. Di Stefano, Unique shape context for 3d data description, in: Proceedings of the ACM workshop on 3D object retrieval, 2010, pp. 57–62.
- [17] D.-Y. Chen, X.-P. Tian, Y.-T. Shen, M. Ouhyoung, On visual similarity based 3d model retrieval, in: *Computer graphics forum*, Vol. 22, Wiley Online Library, 2003, pp. 223–232.
- [18] R. Hänsch, T. Weber, O. Hellwich, Comparison of 3d interest point detectors and descriptors for point cloud fusion, *ISPRS Annals of the Photogrammetry, Remote Sensing and Spatial Information Sciences* 2 (3) (2014) 57.
- [19] H. Ling, D. W. Jacobs, Shape classification using the inner-distance, *IEEE transactions on pattern analysis and machine intelligence* 29 (2) (2007) 286–299.
- [20] Y. Zhou, O. Tuzel, Voxelnet: End-to-end learning for point cloud based 3d object detection, in: Proceedings of the IEEE Conference on Computer Vision and Pattern Recognition, 2018, pp. 4490–4499.
- [21] D. Maturana, S. Scherer, 3d convolutional neural networks for landing zone detection from lidar, in: 2015 IEEE international conference on robotics and automation (ICRA), IEEE, 2015, pp. 3471–3478.

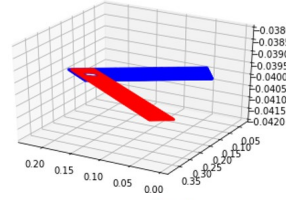
- [22] C. Wang, M. Cheng, F. Sohel, M. Bennamoun, J. Li, Normalnet: A voxel-based cnn for 3d object classification and retrieval, *Neurocomputing* 323 (2019) 139–147.
- [23] S. Ghadai, X. Lee, A. Balu, S. Sarkar, A. Krishnamurthy, Multi-resolution 3d convolutional neural networks for object recognition, arXiv preprint arXiv: 1805.12254 (2018).
- [24] Z. Wu, S. Song, A. Khosla, F. Yu, L. Zhang, X. Tang, J. Xiao, 3d shapenets: A deep representation for volumetric shapes, in: *Proceedings of the IEEE conference on computer vision and pattern recognition*, 2015, pp. 1912–1920.
- [25] H. Su, S. Maji, E. Kalogerakis, E. Learned-Miller, Multi-view convolutional neural networks for 3d shape recognition, in: *Proceedings of the IEEE international conference on computer vision*, 2015, pp. 945–953.
- [26] B. Leng, S. Guo, X. Zhang, Z. Xiong, 3d object retrieval with stacked local convolutional autoencoder, *Signal Processing* 112 (2015) 119–128.
- [27] S. Bai, X. Bai, Z. Zhou, Z. Zhang, L. Jan Latecki, Gift: A real-time and scalable 3d shape search engine, in: *Proceedings of the IEEE conference on computer vision and pattern recognition*, 2016, pp. 5023–5032.
- [28] E. Kalogerakis, M. Averkiou, S. Maji, S. Chaudhuri, 3d shape segmentation with projective convolutional networks, in: *proceedings of the IEEE conference on computer vision and pattern recognition*, 2017, pp. 3779–3788.
- [29] Z. Cao, Q. Huang, R. Karthik, 3d object classification via spherical projections, in: *2017 International Conference on 3D Vision (3DV)*, IEEE, 2017, pp. 566–574.
- [30] L. Zhang, J. Sun, Q. Zheng, 3d point cloud recognition based on a multi-view convolutional neural network, *Sensors* 18 (11) (2018) 3681.
- [31] P.-S. Wang, Y. Liu, Y.-X. Guo, C.-Y. Sun, X. Tong, O-cnn: Octree-based convolutional neural networks for 3d shape analysis, *ACM Transactions on Graphics (TOG)* 36 (4) (2017) 1–11.
- [32] P.-S. Wang, C.-Y. Sun, Y. Liu, X. Tong, Adaptive o-cnn: a patch-based deep representation of 3d shapes, *ACM Transactions on Graphics (TOG)* 37 (6) (2018) 1–11.
- [33] C. R. Qi, H. Su, K. Mo, L. J. Guibas, Pointnet: Deep learning on point sets for 3d classification and segmentation, in: *Proceedings of the IEEE conference on computer vision and pattern recognition*, 2017, pp. 652–660.
- [34] C. R. Qi, L. Yi, H. Su, L. J. Guibas, Pointnet++: Deep hierarchical feature learning on point sets in a metric space, in: *Advances in neural information processing systems*, 2017, pp. 5099–5108.
- [35] R. Klokov, V. Lempitsky, Escape from cells: Deep kd-networks for the recognition of 3d point cloud models, in: *Proceedings of the IEEE International Conference on Computer Vision*, 2017, pp. 863–872.
- [36] Y. Wang, Y. Sun, Z. Liu, S. E. Sarma, M. M. Bronstein, J. M. Solomon, Dynamic graph cnn for learning on point clouds, *Acm Transactions On Graphics (tog)* 38 (5) (2019) 1–12.

- [37] C. Wang, B. Samari, K. Siddiqi, Local spectral graph convolution for point set feature learning, in: Proceedings of the European conference on computer vision (ECCV), 2018, pp. 52–66.
- [38] Z. Zhang, B.-S. Hua, S.-K. Yeung, Shellnet: Efficient point cloud convolutional neural networks using concentric shells statistics, in: Proceedings of the IEEE International Conference on Computer Vision, 2019, pp. 1607–1616.
- [39] W. Han, C. Wen, C. Wang, X. Li, Q. Li, Point2node: Correlation learning of dynamic-node for point cloud feature modeling, arXiv preprint arXiv:1912.10775 (2019).
- [40] S. Van der Walt, J. L. Schönberger, J. Nunez-Iglesias, F. Boulogne, J. D. Warner, N. Yager, E. Gouillart, T. Yu, scikit-image: image processing in python, PeerJ 2 (2014) e453.
- [41] S. Ioffe, C. Szegedy, Batch normalization: Accelerating deep network training by reducing internal covariate shift, arXiv preprint arXiv:1502.03167 (2015).
- [42] N. Srivastava, G. Hinton, A. Krizhevsky, I. Sutskever, R. Salakhutdinov, Dropout: a simple way to prevent neural networks from overfitting, The journal of machine learning research 15 (1) (2014) 1929–1958.

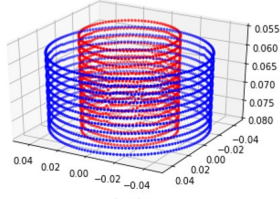
(A)
Expected score: 90-100
Predicted score: 100



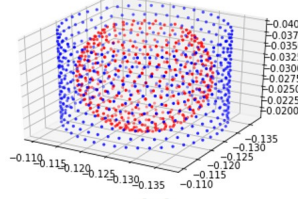
(B)
Expected score: 40-50
Predicted score: 48.5



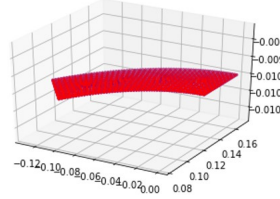
(C)
Expected score: 0-10
Predicted score: 1e-8



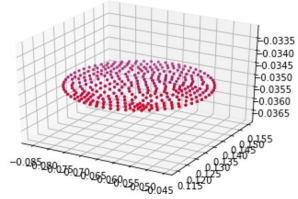
(D)
Expected score: 0-10
Predicted score: 1e-6



(E)
Expected score: 90-100
Predicted score: 100



(F)
Expected score: 90-100
Predicted score: 100



Surface1: blue; Surface2: Red

Figure 8: *ActivationNet* predictions on point clouds of testing geometry 1

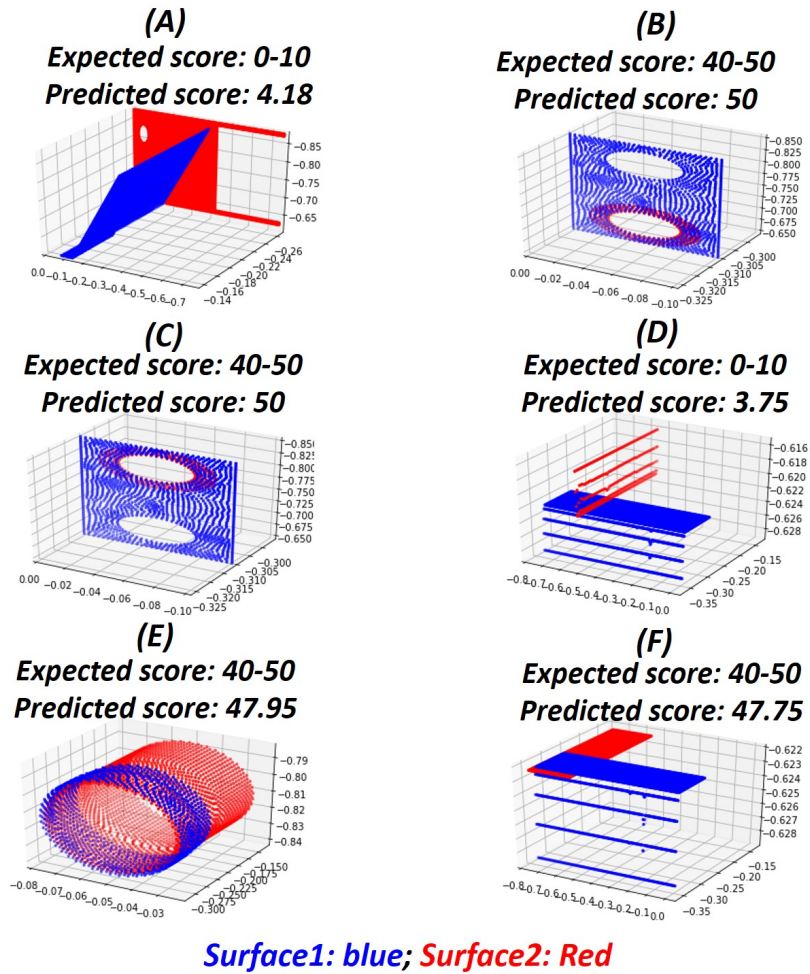


Figure 9: *ActivationNet* predictions on point clouds of testing geometry 2